Tazobactam Forms a Stoichiometric trans -Enamine Intermediate in the E166A Variant of SHV-1 β-Lactamase: 1.63 Å Crystal Structure † , ‡

ARTICLE *in* BIOCHEMISTRY · MARCH 2004

Impact Factor: 3.02 · DOI: 10.1021/bi035985m · Source: PubMed

8 AUTHORS, INCLUDING:

Pius S Padayatti
Rigaku Automation, Carlsbad, CA-92008
20 PUBLICATIONS **815** CITATIONS
SEE PROFILE

Marion S Helfand
Louis Stokes Cleveland VA Medical Center
56 PUBLICATIONS **1,211** CITATIONS
SEE PROFILE

Paul Richard Carey
Case Western Reserve University
75 PUBLICATIONS **1,925** CITATIONS
SEE PROFILE

Accelerated Publications

Tazobactam Forms a Stoichiometric *trans*-Enamine Intermediate in the E166A Variant of SHV-1 β-Lactamase: 1.63 Å Crystal Structure[†,‡]

Pius S. Padayatti,[§] Marion S. Helfand,[||] Monica A. Totir,[⊥] Marianne P. Carey,[§] Andrea M. Hujer,[||] Paul R. Carey,[§,⊥] Robert A. Bonomo,[||] and Focco van den Akker*[,§]

Department of Biochemistry and Department of Chemistry, Case Western Reserve University, Cleveland, Ohio 44106, and Research Division, Louis Stokes Cleveland Veterans Affairs Medical Center, Cleveland, Ohio 44106

Received November 6, 2003

ABSTRACT: Many pathogenic bacteria develop antibiotic resistance by utilizing β-lactamases to degrade penicillin-like antibiotics. A commonly prescribed mechanism-based inhibitor of β-lactamases is tazobactam, which can function either irreversibly or in a transient manner. We have demonstrated previously that the reaction between tazobactam and a deacylation deficient variant of SHV-1 β-lactamase, E166A, could be followed in single crystals using Raman microscopy [Helfand, M. S., *et al*. (2003) *Biochemistry 42,* 13386−13392]. The Raman data show that maximal populations of an enamine-like intermediate occur 20−30 min after "soaking in" has commenced. By flash-freezing crystals in this time frame, we were able to trap the enamine species. The resulting 1.63 Å resolution crystal structure revealed tazobactam covalently bound in the *trans*-enamine intermediate state with close to 100% occupancy in the active site. The Raman data also indicated that tazobactam forms a larger population of enamine than sulbactam or clavulanic acid does and that tazobactam's intermediate is also the most long-lived. The crystal structure provides a rationale for this finding since only tazobactam is able to form favorable intra- and intermolecular interactions in the active site that stabilize this *trans*-enamine intermediate. These interactions involve both the sulfone and triazolyl groups that distinguish tazobactam from clavulanic acid and sulbactam, respectively. The observed stabilization of the transient intermediate of tazobactam is thought to contribute to tazobactam's superior *in vitro* and *in vivo* clinical efficacy. Understanding the structural details of differing inhibitor effectiveness can aid the design of improved mechanism-based β-lactamase inhibitors.

β-Lactamases (EC 3.5.2.6) are in part responsible for the recent surge in antibiotic resistance (*1*, *2*). These enzymes are responsible for degrading and thus eliciting bacterial resistance to the β-lactam antibiotics penicillins and cephalosporins. β-Lactam antibiotics, if left intact, inhibit the final stages of peptidoglycan synthesis, thus killing pathogenic bacteria. To counteract the bacteria's ability to degrade β-lactam antibiotics, a combination treatment of penicillin or cephalosporin with β-lactamase inhibitors is given to patients to combat infections. Currently, the only commonly utilized β-lactamase inhibitors are clavulanic acid, sulbactam, and tazobactam (*3*). These inhibitors form a covalent acyclic linear molecule during its reaction with β-lactamase and can inhibit both in a transient and irreversible manner (*4*). Unfortunately, by undergoing single amino acid substitutions. β-lactamases often themselves become resistant to inhibition.

β-Lactamases have been classified into four groups (A−D). Members of the clinically prevalent class A are SHV-1, SHV-2, and TEM-1, of which numerous variants with altered activity have been isolated (*1*). To aid in the further development of potent β-lactamase inhibitors, the catalytic mechanism of class A β-lactamases has been studied intensely. Our knowledge of the β-lactamase reaction mechanism is based on the work of Knowles (*5*−*13*) and others (*14*, *15*). This reaction scheme was later extended to tazobactam (*16*, *17*) (Figure 1). The initial step is an enzyme-induced strain in the ligand (*18*) followed by the involvement of S70 in forming a covalent acyl intermediate. Several reaction intermediates involving clavulanic acid and tazobactam have been visualized using cryoprotein crystallography (*19*, *20*). However, these were obtained by soaking or cocrystallization experiments without prior knowledge of which intermediate was trapped or when the best time point is to trap a specific intermediate. Raman spectroscopy on

[†] M.S.H. and R.A.B. are supported by the Department of Veterans Affairs Career Development Award program and the Merit Review Program, respectively. P.R.C. is supported by NIH Grant GM54072. F.v.d.A. is supported by a SDG grant from the American Heart Association and NIH Grant DK65066.

[‡] The coordinates and structure factors are deposited with the Protein Data Bank (entry 1RCJ).

* To whom correspondence should be addressed: Department of Biochemistry RT500, School of Medicine, Case Western Reserve University, 10900 Euclid Ave., Cleveland, OH 44106-4935. Phone: (216) 368-8511. E-mail: focco.vandenakker@case.edu.

[§] Department of Biochemistry, Case Western Reserve University.

[||] Louis Stokes Cleveland Veterans Affairs Medical Center.

[⊥] Department of Chemistry, Case Western Reserve University.

10.1021/bi035985m CCC: $27.50
Published on Web 01/03/2004

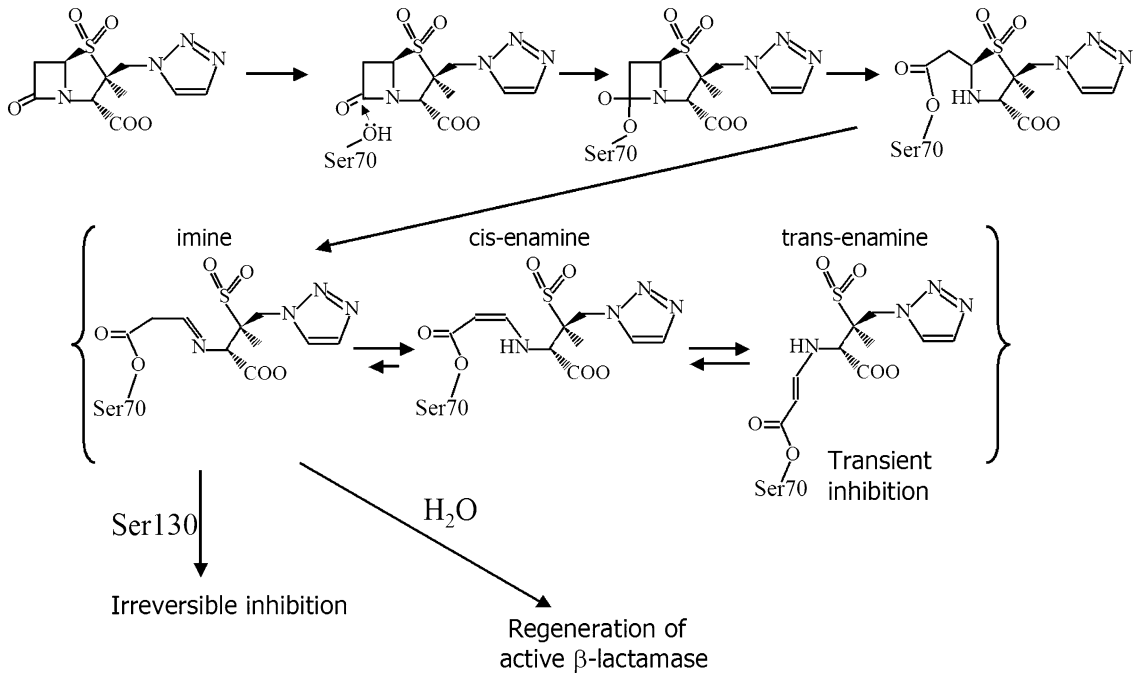

FIGURE 1: Proposed reaction scheme for tazobactam with β-lactamases. The transient inactivation of SHV-1 involves the *trans*-enamine intermediate which is more energetically favorable than the *cis*-enamine intermediate.

protein crystals has recently emerged as an elegant tool for tracking the intermediates of reactions in protein crystals (*21*, *22*).

The β-lactamase E166A variant is particularly useful since deacylation is no longer catalyzed and the acyl enzyme is hydrolyzed very slowly. This allows us to focus on the acylation part of the reaction and, in particular, on the covalently bound intermediate. Monitoring the reaction of tazobactam within a E166A β-lactamase crystal with Raman spectroscopy revealed the formation of an enamine intermediate peaking around 20−30 min after the start of the soaking experiment. More of this intermediate appeared to form with tazobactam than with sulbactam or clavulanic acid (*22*). We thus targeted the tazobactam-based intermediate for crystallographic study. This novel combined spectroscopic and cryocrystallographic approach enables us to provide the first high-resolution structure of a labile β-lactamase tazobactam intermediate where virtually all molecules have been trapped as a single uniform species on the reaction pathway.

MATERIALS AND METHODS

The E166A variant of SHV-1 β-lactamase was expressed and purified as described previously (*22*).

Crystallization and Soaking. Crystals were prepared using the sitting drop method as described previously for the wild-type protein (*19*). Drops with a volume of 10 μL were prepared using 4 μL of protein solution, 1 μL of 5.6 mM Cymal-6 (Hampton Research), and 5 μL of 30% (w/v) PEG-6000 in 0.1 M HEPES (pH 7.0). The reservoir solution consisted of 30% (w/v) PEG-6000 in 0.1 M HEPES (pH 7.0). Wells were sealed and stored at room temperature, and crystals grew to full size in 2−3 days. For the soaking experiments, the E166A crystals were transferred to 10 μL drops containing 30% PEG-6000 in 0.1 M HEPES (pH 7.0) with 0.56 mM Cymal-6 and 5 mM tazobactam for 20−25 min, determined previously by Raman spectroscopy to be the optimal concentration and time point for observing the intermediate (*22*). Immediately after this soak, the crystals were cryoprotected in mother liquor containing 25% 2-methyl-2,4-pentanediol (MPD) for 1−2 min and flash-cooled via immersion in liquid nitrogen using a cryoloop. Data were collected with the crystal cooled in a gaseous nitrogen stream at −170 °C, using an in-house Rigaku rotating-anode generator (Molecular Structure Corp.) equipped with Yale mirrors, and an R-AXIS IV image plate detector. Data processing was carried out with SCALEPACK and DENZO (*23*) (Table 1).

Table 1: Data Collection and Refinement Statistics

data collection	
space group	$P2_12_12_1$
unit cell dimensions (Å)	$a = 49.8$, $b = 55.2$, $c = 83.9$
wavelength (Å)	1.54
resolution (Å)	30−1.63 (1.69−1.63)
redundancy	4.3
no. of unique reflections	28328
$\langle I\rangle/\langle\sigma(I)\rangle$	40.49 (12.6)
R_{merge} (%)	3.2 (8.0)
completeness (%)	95.6 (87.7)
refinement	
resolution range (Å)	30−1.63
R-factor (%)	14.7
R_{free} (%)	17.2
rms deviations from ideality	
bond lengths (Å)	0.0088
bond angles (deg)	1.58

Crystallographic Refinement. Structure determination was carried out using the crystal structure of wild-type SHV-1 β-lactamase with bound tazobactam (PDB entry 1G56) (*19*) since its crystal is isomorphous with that of the E166A mutant. The program CNS (*24*) was used for crystallographic refinement. The wild-type protein coordinates with the E166 side chain truncated to alanine and all inhibitor, solvent, and other ligand atoms removed provided the starting model. An initial rigid body refinement was followed by model mini-

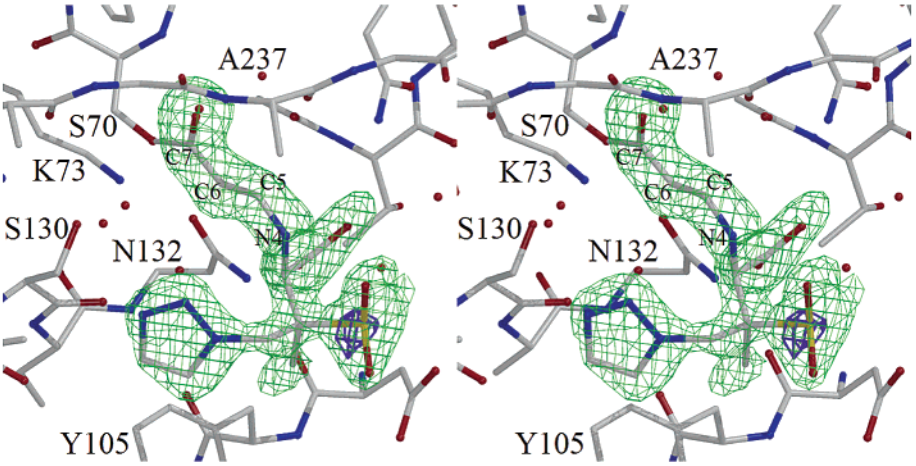

FIGURE 2: Electron density of tazobactam bound to the E166A mutant of SHV-1 β-lactamase. The omit electron density (green) for the tazobactam ligand is contoured at 2.8σ, and the anomalous difference Fourier electron density map (purple) is contoured at 4σ. The *trans*-enamine bond involves the C5 and C6 atoms of the tazobactam intermediate.

mization, temperature factor refinement, and simulated annealing. After several rounds of refinement, the tazobactam and Cymal-6 molecules were placed into difference density and included in additional rounds of refinement. Throughout the calculations, an overall anisotropic *B*-factor was applied in CNS. Refinement topology and parameter files for tazobactam were generated using the PRODRG2 server (*25*), and interactive graphical model rebuilding with O (*26*) was carried out between refinement cycles. The progress of crystallographic refinement was monitored using the programs DDQ (*27*) and PROCHECK (*28*).

RESULTS

The final refined model of the E166A variant of SHV-1 β-lactamase bound to tazobactam contains residues 26−292, a covalently bound *trans*-enamine tazobactam, a Cymal-6 molecule, and 300 water molecules. Refinement against diffraction data to 30−1.63 Å resolution yielded an *R*-factor of 14.7% and an R_{free} of 17.1%. The DDQ program is able to rank the quality of a crystal structure with respect to other structures in the Protein Data Bank determined at a similar resolution. The E166A−tazobactam structure received a DDQ-R ranking of "Top 25%" for its score of 82.8 (*27*) (Table 1). Nearly all (92.6%) of the residues fall within the most favored core of the Ramachandran plot, and none are within the disallowed region. Nine residues were modeled with alternative conformations.

The crystal structure of the deacylation deficient E166A variant of SHV-1 β-lactamase is very similar overall to that of the wild-type except for flexible C-terminal residues 291 and 292. The root-mean-square deviation for the Cα atoms of residues 26−290 is 0.47 Å between the E166A and wild-type SHV-1 β-lactamase. The most important differences are in the active site, in particular in the Ω loop containing the site of the mutation; these differences will be discussed later.

Tazobactam Conformation. The electron density for the covalently bound tazobactam is well-defined for the carboxylate moiety, the sulfone group, the methyl group, and the triazolyl ring (Figure 2).

The tazobactam in the E166A structure is clearly a *trans*-enamine intermediate since the torsion angles about the C5−C6 bond refined to 168° (the torsion angle about the N4−C5 bond is 5°). The covalently bound tazobactam in our E166A structure is a species quite different from the imine structure observed in the wild-type structure (*19*), the details of which are discussed below. To confirm the correct positioning of the sulfone group, an anomalous difference Fourier electron density map was calculated. At the 1.542 Å wavelength used for data collection, sulfur atoms exhibit significant anomalous scattering. The sulfur of the tazobactam sulfone moiety corresponds to a 6.0σ peak in the anomalous difference map, confirming that the inhibitor has been modeled correctly (Figure 2). For comparison, the sulfurs of the deeply buried Met and Cys residues in the protein structure yielded anomalous difference peaks of 9.9−17.2σ. In contrast to the wild-type tazobactam findings, no noncovalently bound tazobactam was observed in our E166A structure. This is likely due to the much lower soaking concentrations used here (5 mM) compared to that used in the experiments for the wild-type structure (tazobactam concentration of 42 mM). To estimate the occupancy of the tazobactam after the 20 min soak, we carried out refinements with the tazobactam at occupancies of 0.8, 0.9, and 1.0, and compared the resulting temperature factors of the bonded S70 Oγ atom and the O7 atom of tazobactam (note that at this resolution, one cannot refine occupancy and temperature factors since these two parameters are highly correlated). The temperature factors of the bonded atoms refined to within a few square angstroms of each other for both the occupancies of 0.9 and 1.0, so we estimate the tazobactam occupancy at >90% and kept the occupancy at 1.0 during the refinement. The occupancy of the tazobactam bound to S70 in the wild-type structure was 0.5 (*19*).

DISCUSSION

Overall, the protein structure of the SHV-1 β-lactamase E166A variant with tazobactam bound is similar to that of the corresponding complex with the wild-type protein. However, a closer comparison of the structures reveals two highly significant differences, in the nature of the species formed from tazobactam and at the site of the E166A mutation. These will be discussed in detail below, whereas differences such as the E166A structure's lack of the S130 modification and the absence of noncovalently bound tazobactam will be discussed only briefly .

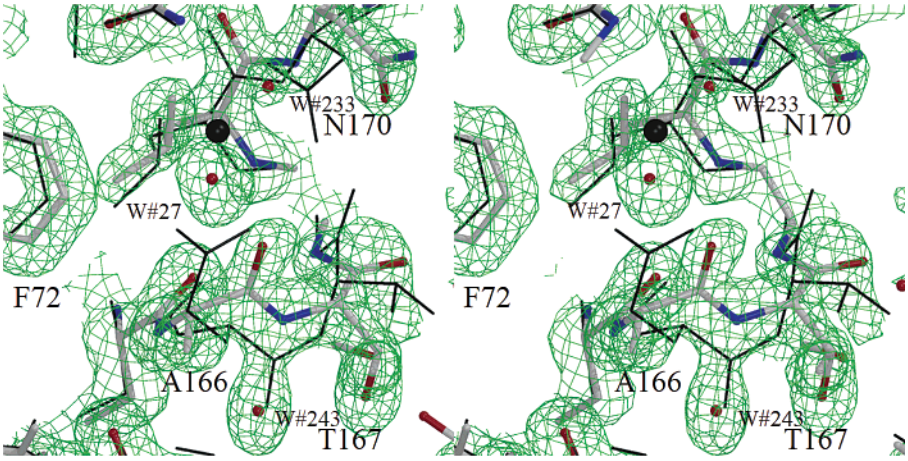

FIGURE 3: Stereoview of the mutated residue A166. Shown are the wild-type structure (black lines) and its E166-activated water (black sphere), superimposed on the E166A structure (colored ball-and-stick diagram) and its corresponding $2|F_o| - |F_c|$ density contoured at 1σ. Two new waters are observed in the E166A structure (waters 27 and 233). A166 has undergone a peptide flip, with a solvent molecule (water 243) occupying the position of the E166 carbonyl in the wild-type structure forming a 2.5 Å hydrogen bond with the backbone nitrogen of T167.

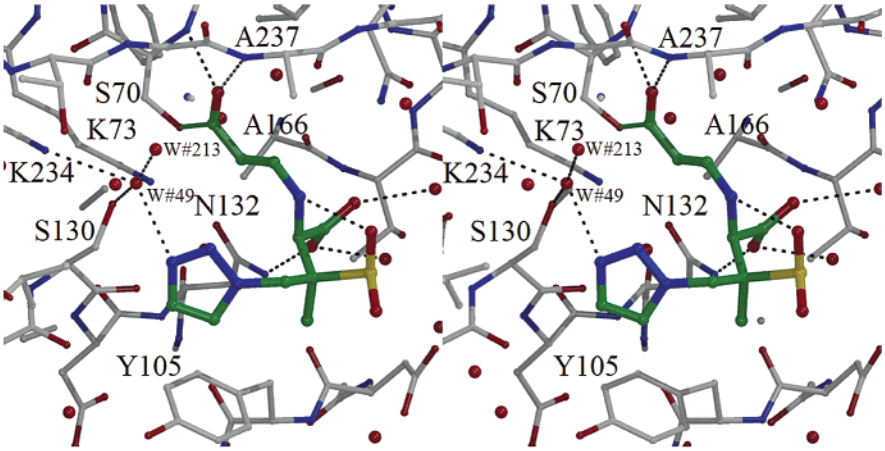

FIGURE 4: Tazobactam bound to the E166A structure of SHV-1 β-lactamase. Tazobactam (thick bonds and green carbon atoms) is covalently bound to S70 and forms both intramolecular and intermolecular hydrogen bond interactions (dashed lines).

One significant difference in the protein structure is found in the Ω loop which harbors the mutation site at position 166. A peptide flip has occurred at residue E166A (Figure 3); the backbone carbonyl oxygen is replaced with a water molecule that forms a 2.5 Å hydrogen bond with the backbone nitrogen of T167. In addition to the E166A peptide flip, the neighboring T167 has shifted ~1.5 Å and makes a 2.7 Å hydrogen bond with the new water. In the wild-type enzyme, the E166 side chain has recently been identified as the base that may activate the water molecule which is involved in both the acylation and deacylation reactions of the S70 residue (*29*, *30*). This water is normally held in place by the E166 and N170 side chains (*29*, *30*).

In our E166A SHV crystal structure, the smaller E166A side chain creates space for the normally catalytic water to move 1.2 Å, making room for a second water ~2.8 Å away (Figure 3). N170 has swung out from its normal position in which it hydrogen bonds with the wild-type catalytic water, also to make room for the second active site water. Although these local changes in the Ω loop are intriguing, the likely reason for the inactivity of the E166A enzyme is still the loss of the critical base E166. Crystal structures of Toho-1 and *Bacillus licheniformis* β-lactamases with the E166A and their wild-type counterpart have been published (*31*−*33*). In the other two enzymes, the E166A mutation also causes little change in protein conformation except for the loss of the catalytic base. The peptide flip observed in our SHV-1 structure is not possible in the latter β-lactamases since they both have a proline at residue 167 which limits the flexibility of the peptide bond between residues 166 and 167.

Tazobactam Interactions. The covalently bound compound formed from tazobactam participates in a number of interactions with the protein in addition to forming an intramolecular interaction (Figures 4 and 5).

The O8 atom of tazobactam is located in an oxyanion hole and is stabilized by hydrogen bonds with the backbone NH atoms of residues 70 and 237. The inhibitor's carboxylate moiety forms a 2.7 Å hydrogen bond with the Nδ2 atom of N132. The tazobactam triazolyl moiety's N17 nitrogen atom makes a 2.7 Å hydrogen bond with water 49 which is deeply buried within the active site, and which is involved in additional interactions with K234 and S130. In addition to this hydrogen bond, the triazolyl moiety is also involved in hydrophobic interactions with Y105. Finally, the methyl group of tazobactam is making hydrophobic interactions with Y105. In addition to these intermolecular interactions, tazobactam also contains an intramolecular interaction; the oxygen of the sulfone group forms a 2.8 Å hydrogen bond

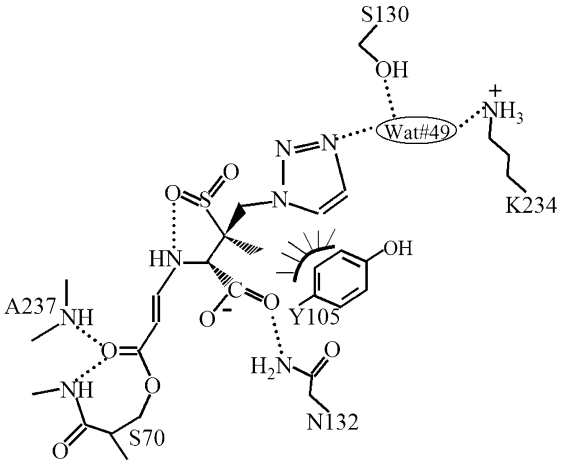

FIGURE 5: Schematic diagram of tazobactam bound to the E166A mutant of SHV-1 β-lactamase. Hydrogen bonds are highlighted as dotted lines, and the hydrophobic van der Waals interactions between Y105 and the triazolyl ring and methyl moieties of tazobactam are depicted by a curved line with perpendicular stripes. The carboxyl moiety interactions with two weakly bound water molecules at the perimeter of the active site as shown in Figure 4 are omitted for clarity.

with the N4 atom. Because of the *trans*-enamine configuration, this nitrogen contains a hydrogen and is thus capable of making the interaction. This intramolecular hydrogen bond thus provides further evidence that the bound tazobactam is not the imine intermediate since the necessary hydrogen atom is absent in the imine intermediate.

Tazobactam Species Formed in Wild-Type and Mutant Complexes. The tazobactam *trans*-enamine intermediate found bound to the deacylation deficient SHV-1 E166A mutant is of interest since it is quite different from the imine intermediate previously observed in the wild-type structure (*19*) (Figure 6).

Superposition and comparison of the two structures reveal a possible explanation for the difference in inhibitor conformation. The wild-type enzyme is not deacylation deficient, and during the soaking time of 6 h, it undergoes many reaction cycles and accumulates an additional reaction intermediate in which S130 is covalently modified with vinylcarboxylic acid, one of the possible end products of the reaction. This S130 modification could only be observed when the crystals were soaked with high millimolar tazobactam concentrations and appeared only after 6 h of soaking (*19*). The bulky S130 modification, which occurred with an occupancy of 100%, narrows the active site and therefore sterically hinders the tazobactam residue attached to S70, disfavoring it from adopting the *trans*-enamine conformation (Figure 6). When the entire wild-type and E166A structures are superimposed, the carboxyl atom of the vinyl carboxylic is within 3.10 Å of the C5 atom of the putative *trans*-enamine conformation (2.9 Å if only the residues around positions 70 and 130 are used for the superpositioning). This short distance is sterically unfavorable, and the C5 atom of tazobactam in the wild-type structure must shift to accommodate the modified S130 by increasing the distance to 4.0 Å. The steric restrictions on the C5 atom appear to result in the inability of the inhibitor to adopt the *trans*-enamine intermediate in the presence of a covalently modified S130. Furthermore, the *trans*-enamine intermediate was also observed in compounds similar to tazobactam bound to the *C. freundii* class C β-lactamase (*34*), and a mixture of *cis*- and *trans*-enamine was observed for clavulanic acid bound to *Streptomyces aureus* class A β-lactamase (*20*).

Correlation with Raman Spectroscopy. The E166A mutant of SHV-1 β-lactamase is an ideal candidate for studying the reaction intermediates using spectroscopy or crystallography, as the deacylation deficient enzyme favors the accumulation of acyl enzymes. The Raman data for the three inhibitors reacting with β-lactamase reveal the presence of the *trans*-enamine intermediate, albeit at different population levels and with different half-lives. Tazobactam forms approximately 50% more of this intermediate than sulbactam does, and clavulanic acid forms slightly less *trans*-enamine intermediate that sulbactam (*22*). The half-life for the *trans*-enamine intermediate is also the longest for tazobactam. The relative ability of tazobactam, sulbactam, and clavulanic acid (from best to worst) in forming the *trans*-enamine intermediate is intriguing and can be explained by the E166A complex structure. The tazobactam sulfone group forms an intramolecular 2.8 Å hydrogen bond with its N4 atom (Figure 4) which is only possible in the enamine intermediate where this nitrogen is protonated, and not in the imine intermediate where it is deprotonated (see Figure 1). The observation of

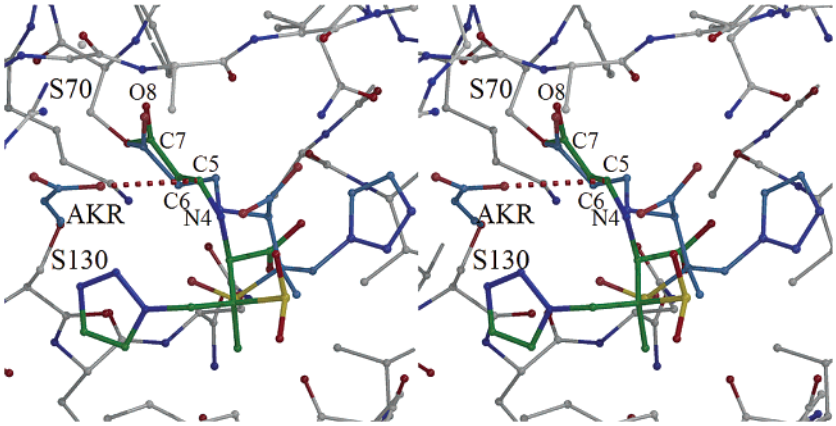

FIGURE 6: Tazobactam bound to wild-type and E166A SHV-1 β-lactamase. Shown are tazobactam in its conformation when bound to the E166A protein (green carbon atoms) and when bound to the wild-type enzyme (blue carbon atoms), with the E166A protein structure (thin bonds). In the wild-type structure, Ser130 is modified with an acrylic acid group (AKR, thick bonds), which sterically interferes (red dashed line) with the C5 atom of the *trans*-enamine tazobactam conformation observed in the E166A complex. Instead, the bulkier modified S130 pushes the tazobactam C5 atom back, thus favoring the imine over the *trans*-enamine intermediate.

this *trans*-enamine-stabilizing hydrogen bond is consistent with tazobactam and sulbactam forming much more of the *trans*-enamine intermediate than clavulanic acid, since the sulfone moiety is present only in the first two compounds. The most significant difference between tazobactam and sulbactam lies in the presence of a triazolyl moiety in the former, whereas the latter has a methyl group attached to the C2 atom. In the E166A structure, the triazolyl N17 atom makes a 2.7 Å hydrogen bond with a buried water molecule (water 49), which in turn forms additional hydrogen bonds with S130 Oδ, K234 Nζ, and another water (water 213). In addition, the triazolyl moiety forms a favorable van der Waals interaction with Y105. These interactions appear to stabilize the *trans*-enamine tazobactam intermediate but are not possible in the triazolyl deficient sulbactam.

Our structural explanation for the relative *trans*-enamine forming tendency of tazobactam, sulbactam, and clavulanic acid (from strongest to weakest) is especially interesting in light of the fact that the clinical efficacy of these inhibitors is in the same order, with tazobactam being the most potent (*35*). Successful inhibition of β-lactamases may be a combination of both transient and irreversible inhibition (*4*). It is tempting to speculate that the intra- and intermolecular interactions discussed above may play a role in tazobactam's superior *in vitro* inhibitory activities (*36*) and clinical efficacy (*35*). Despite this attractive explanation, we do keep in mind that other mechanisms might occur such as loss of the sulfone group with a concomitant molecular rearrangement (*34*).

The interplay of Raman crystallography and protein crystallography is emerging as a powerful combination for probing molecular structure and function relationships. Because of the relatively slow time scale of the reaction, the Raman technique identified the tazobactam-based *trans*-enamine intermediate and provided a means of tracking the progress of the reaction inside a crystal. This allowed us to chose the optimal time at which to stop the reaction by cryocooling the tazobactam-soaked crystal. To our knowledge, this is the first example of such a Raman-assisted controlled soaking experiment for trapping a reaction intermediate inside a crystal. We anticipate that other protein enzyme crystal systems could be amenable to this combined approach. Reactions that proceed on the order of minutes are desired since currently Raman measurements can be taken only every 90 s.

Our structure of the tazobactam bound to the E166A variant of SHV-1 β-lactamase may be of considerable interest in designing improved clinical inhibitors by further stabilizing the *trans*-enamine intermediate. These studies reveal intra- and intermolecular interactions involving the sulfone and triazolyl moieties of tazobactam that may be important factors contributing to its behavior as a better β-lactamase inhibitor than sulbactam and clavulanic acid.

ACKNOWLEDGMENT

We thank Vivien Yee for critical reading of the manuscript.

REFERENCES

1. Helfand, M. S., and Bonomo, R. A. (2003) *Curr. Drug Targets: Infect. Disord. 3*, 9−23.
2. Bush, K. (2002) *Curr. Opin. Invest. Drugs 3*, 1284−1290.
3. Lee, N., Yuen, K. Y., and Kumana, C. R. (2003) *Drugs 63*, 1511−1524.
4. Therrien, C., and Levesque, R. C. (2000) *FEMS Microbiol. Rev. 24*, 251−262.
5. Charnas, R. L., Fisher, J., and Knowles, J. R. (1978) *Biochemistry 17*, 2185−2189.
6. Brenner, D. G., and Knowles, J. R. (1981) *Biochemistry 20*, 3680−3687.
7. Brenner, D. G., and Knowles, J. R. (1984) *Biochemistry 23*, 5839−5846.
8. Brenner, D. G., and Knowles, J. R. (1984) *Biochemistry 23*, 5833−5839.
9. Charnas, R. L., and Knowles, J. R. (1981) *Biochemistry 20*, 3214−3219.
10. Fisher, J., Charnas, R. L., and Knowles, J. R. (1978) *Biochemistry 17*, 2180−2184.
11. Fisher, J., Charnas, R. L., Bradley, S. M., and Knowles, J. R. (1981) *Biochemistry 20*, 2726−2731.
12. Fisher, J., Belasco, J. G., Khosla, S., and Knowles, J. R. (1980) *Biochemistry 19*, 2895−2901.
13. Fisher, J., Belasco, J. G., Charnas, R. L., Khosla, S., and Knowles, J. R. (1980) *Philos. Trans. R. Soc. London, Ser. B 289*, 309−319.
14. Brown, R. P., Aplin, R. T., and Schofield, C. J. (1996) *Biochemistry 35*, 12421−12432.
15. Bonomo, R. A., Liu, J., Chen, Y., Ng, L., Hujer, A. M., and Anderson, V. E. (2001) *Biochim. Biophys. Acta 1547*, 196−205.
16. Bush, K., Macalintal, C., Rasmussen, B. A., Lee, V. J., and Yang, Y. (1993) *Antimicrob. Agents Chemother. 37*, 851−858.
17. Yang, Y., Janota, K., Tabei, K., Huang, N., Siegel, M. M., Lin, Y. I., Rasmussen, B. A., and Shlaes, D. M. (2000) *J. Biol. Chem. 275*, 26674−26682.
18. Hokenson, M. J., Cope, G. A., Lewis, E. R., Oberg, K. A., and Fink, A. L. (2000) *Biochemistry 39*, 6538−6545.
19. Kuzin, A. P., Nukaga, M., Nukaga, Y., Hujer, A., Bonomo, R. A., and Knox, J. R. (2001) *Biochemistry 40*, 1861−1866.
20. Chen, C. C., and Herzberg, O. (1992) *J. Mol. Biol. 224*, 1103−1113.
21. Carey, P. R. (1999) *J. Biol. Chem. 274*, 26625−26628.
22. Helfand, M. S., Totir, M. A., Carey, M. P., Hujer, A. M., Bonomo, R. A., and Carey, P. R. (2003) *Biochemistry 42*, 13386−13392.
23. Otwinowski, Z., and Minor, W. (1997) *Methods Enzymol. 276*, 307−326.
24. Brunger, A. T., Adams, P. D., Clore, G. M., DeLano, W. L., Gros, P., Grosse-Kunstleve, R. W., Jiang, J. S., Kuszewski, J., Nilges, M., Pannu, N. S., Read, R. J., Rice, L. M., Simonson, T., and Warren, G. L. (1998) *Acta Crystallogr. D54*, 905−921.
25. van Aalten, D. M., Bywater, R., Findlay, J. B., Hendlich, M., Hooft, R. W., and Vriend, G. (1996) *J. Comput.-Aided Mol. Des. 10*, 255−262.
26. Jones, T. A., Zou, J. Y., Cowan, S. W., and Kjeldgaard (1991) *Acta Crystallogr. A47* (Part 2), 110−119.
27. van den Akker, F., and Hol, W. G. (1999) *Acta Crystallogr. D55* (Part 1), 206−218.
28. Laskowski, R. A., MacArthur, M. W., Moss, D. S., and Thornton, J. M. (2001) *J. Appl. Crystallogr. 26*, 283−291.
29. Nukaga, M., Mayama, K., Hujer, A. M., Bonomo, R. A., and Knox, J. R. (2003) *J. Mol. Biol. 328*, 289−301.
30. Minasov, G., Wang, X., and Shoichet, B. K. (2002) *J. Am. Chem. Soc. 124*, 5333−5340.
31. Knox, J. R., Moews, P. C., Escobar, W. A., and Fink, A. L. (1993) *Protein Eng. 6*, 11−18.
32. Ibuka, A., Taguchi, A., Ishiguro, M., Fushinobu, S., Ishii, Y., Kamitori, S., Okuyama, K., Yamaguchi, K., Konno, M., and Matsuzawa, H. (1999) *J. Mol. Biol. 285*, 2079−2087.
33. Ibuka, A. S., Ishii, Y., Galleni, M., Ishiguro, M., Yamaguchi, K., Frere, J. M., Matsuzawa, H., and Sakai, H. (2003) *Biochemistry 42*, 10634−10643.
34. Richter, H. G., Angehrn, P., Hubschwerlen, C., Kania, M., Page, M. G., Specklin, J. L., and Winkler, F. K. (1996) *J. Med. Chem. 39*, 3712−3722.
35. Page, M. G. (2000) *Drug Resist. Updates 3*, 109−125.
36. Yang, Y., Rasmussen, B. A., and Shlaes, D. M. (1999) *Pharmacol. Ther. 83*, 141−151.

BI035985M